Surface structure, morphology and (110) twin of aragonite

UNIVERSITÀ DEGLI STUDI DI TORINO

Surface structure, morphology and (110) twin of aragonite

Francesco Roberto Massaro[1]* *Marco Bruno*[2] *Marco Rubbo*[2]

[1]Dipartimento di Geoscienze – Università di Padova, via G. Gradenigo 6, I-35131 Padova, Italy

[2]Dipartimento di Scienze della Terra - Università di Torino, via Valperga Caluso 35, I-10125 Torino, Italy.

* *Corresponding author*
e-mail: francescoroberto.massaro@unipd.it
Tel.: +390116705140
Fax: +390116705128

Abstract

In order to better understand the growth mechanisms involving the aragonite in both geological and biological systems, a detailed study of its surfaces was performed. By adopting a two dimensional slab model and performing empirical calculations, we determined the equilibrium geometry at 0K of the (100), (010), (001), (110), (101), (011), (111), (102), (012), (021), (112), (121), (122), (031) and (130) surfaces, both in anhydrous and hydrated conditions. Furthermore, the equilibrium geometry at 0K of the (110) twin boundary interface was also determined.

The dry and solvated surface energies at 0K of the crystal faces were also calculated, as well as the (110) twinning energy at 0K, a key thermodynamical quantity for the determination of the equilibrium morphology of twins, and the estimation of their most probable mechanism of formation during growth. As concerns the (110) twin, the interface elastic energy was also evaluated.

The solvated equilibrium shape (ES) of aragonite is drawn and compared to the dry one; a comparison with the previous dry and solvated ES calculated at 0K is also performed. Furthermore, the surface structure modifications due to the presence of water is discussed.

Our calculations explain the high occurrence of twinned crystals in case of nucleation and growth in inorganic environments. On the contrary, in living organism the crystallization route, the crystal sizes and morphologies are deeply modified by the adhesion on organic substrates and adsorption of organic molecules.

1. Introduction

Aragonite (space group *Pmcn*; $a_0 = 4.9614$, $b_0 = 7.9671$, $c_0 = 5.7404$ Å; $\alpha = \beta = \gamma = 90°$)[1] is one of the two common, naturally occurring polymorphs of the calcium carbonate ($CaCO_3$) (the other one is calcite) found in geological and biological systems. In particular, aragonite is the main component of nacre (mother-of-pearl) that is found in the innermost part of many mollusk shells. Indeed, nacre is composed of approximately 95 vol.% brittle inorganic aragonite and a small percentage of organic biopolymer.[2] This material has a brick-and-mortar-like structure with highly organized polygonal aragonite platelets of a thickness ranging from 200 to 500 nm and an edge length of about 5 μm sandwiched with a 5–20 nm thick organic biopolymer interlayer, which assembles the aragonite platelets together.[3]

Recently, it has been shown by means of high resolution TEM images and electronic diffraction that single-crystal-like aragonite platelets of *Haliotis rufescens*, *Haliotis discus hannai* and *Omphalius rusticus* (belonging to the class of gastropoda) are essentially assembled with aragonite nanoparticles with very similar crystallographic orientation.[4,5] The unique crystal structure of aragonite and the arrangement of the aragonite nanoparticles in nacre's platelets make the diffraction patterns of individual platelets exhibit single-crystal characteristics.[4,5] AFM observations on *Haliotis rufescens* and *Pinctada maxima* (a giant oyster) have also shown that individual aragonite platelets consist of a large number of nanoparticles.[3,6,7]

Interestingly, the aragonite nacre's platelets analysed in the works above cited do not show heavy {110} twinning, which was instead observed into other shell structures[8] and into acicular aragonite crystals forming the fibrous layer between the inner nacreous and outer calcite layers of *Haliotis discus hannai* and *Omphalius rusticus*.[4,5] Instead, simple aragonite crystals of inorganic origin are rare, as twinning about the 110 plane is nearly always present. When the triplet twinning occurred (i.e., repeated twinning about the 110 plane), the resulting crystal becomes pseudo-hexagonal, which is almost indistinguishable from simple hexagonal one.

Furthermore, it is interesting to note that growing aragonite crystals from the nacre of some mollusks are round, while aragonite crystals produced by other species of mollusks are polygonal in shape. A beautiful example of such a morphological difference is reported by Mukai et al.,[4] which observed pseudo-hexagonal aragonite tablets (composed by the {110}, {010} and {001} forms) in *Haliotis discus hannai* and platelets with elliptical shape in *Omphalius rusticus*, where the only recognizable crystallographic form is the {001}. As reported by Wada,[9] these morphological differences may be either seasonal or intrinsic of each species. However, in both cases the

morphology of the crystals should be dictated by the interaction between organic matter (interlamellar organic sheet) and the aragonite crystals growing inside it. Indeed, TEM studies of the growing nacre have demonstrated that the interlamellar matrix is formed prior to mineral deposition.[10] This means that the aragonite crystals nucleate and grow in a preformed compartment composed by organic matter, which should be able to facilitate the formation of aragonite crystals with a peculiar growth shape (i.e., tabular habit), completely different from that observed in aragonite crystals of inorganic origin, where a prismatic or acicular (needle-like) habit is usually displayed. The pseudo-hexagonal tabular morphology of the biogenic crystals in nacre is probably a consequence of the preferential adsorption of the organic matter on the {001} form with respect to the {110} and {010} ones. Indeed, this adsorption selectivity should entail a lower growth rate of the {001} faces than those of the {110} and {010} faces, with consequent formation of a tabular growth shape.

The determination of the most probable surface structure is of fundamental importance to gain more insights on impurities adsorption, epitaxy and twinning. Indeed, the modelling and interpretation of such phenomena require the knowledge of the structure of the interface on which the phenomenon occurs. Therefore, in order to better understand the growth mechanisms involving the aragonite in both geological and biological systems, a detailed study of its surfaces is essential. Interestingly, at variance with the case of calcite (see Bruno et al.[11] and references therein), a very few computational studies on the surfaces of the aragonite were until now performed.[12-15] In addition, only one of these papers took into account the effect of the water on the structural modification of the crystal faces.[14]

Therefore, in order to gain more insights on the structure and energy of the crystal faces of aragonite, in this work, by adopting a two dimensional slab model and performing empirical calculations, we aimed at the determination of the equilibrium geometry at 0K of the (100), (010), (001), (110), (101), (011), (111), (102), (012), (021), (112), (121), (122), (031) and (130) surfaces, both in anhydrous (dry) and hydrated (solvated) conditions. Furthermore, the equilibrium geometry at 0K of (110) twin boundary interface was also determined. We decided for empirical calculations since, due to the complexity of our system, the quantum-mechanical approach would be too demanding.

The dry and solvated surface energies at 0K of the (100), (010), (001), (110), (101), (011), (111), (102), (012), (021), (112), (121), (122), (031) and (130) faces were also calculated, as well as the (110) twinning energy at 0K (the work required to form a unit area of the twin interface), a key thermodynamical quantity for the determination of the equilibrium morphology of twins, and the

estimation of their most probable mechanism of formation during growth. As concerns the (110) twin, the elastic energy was also evaluated.

In order to determine the equilibrium geometries of solvated crystal faces and solvated surface energies at 0K, the COSMIC method[16] was applied. Then, the solvated equilibrium shape (ES) of aragonite is drawn and compared to the dry one; a comparison with the previous dry and solvated ES calculated at 0K is also performed. Furthermore, the surface structure modifications due to the presence of water is discussed. In order to estimate how our results are affected by the COSMIC parameters, we tested the algorithm by using different computational parameters. As in the case of calcite,[11] we will show that different choices of the COSMIC parameters do not affect significantly the surface structures and the ES at 0K of aragonite. At the best of our knowledge, these are the first COSMIC calculations performed on the aragonite surfaces.

The structure of the paper is as follows: (1) description of the computational parameters used to determine the equilibrium geometry of the crystal surfaces and twinning interface; (2) presentation of the results, together with their interpretation; (3) main conclusions and perspectives.

2. Computational details

Calculations (optimizations of slab geometries, dry and solvated surface energies and twinning energy estimates) were performed by using the inter-atomic potential for calcite developed by Rohl et al.[17] (Rohl potential hereinafter). The solvated equilibrium geometries and solvated surface energies were obtained by using the COSMIC model,[16] which is implemented in the 4.0 release of GULP (General Utility Lattice Program) simulation code,[18] a computational program based on force field methods allowing the calculation of structures and properties of minerals from a given set of empirical potentials.

The parameters of the Rohl potential were obtained by fitting structural data for both calcite and aragonite, as well as physical properties (elastic and dielectric constants) and phonon frequencies. The COSMIC model allows the calculation of the solvation energy at T=0K of a 2D periodic system like a surface; it is an extension of the well-established COSMO solvation model.[19] Calculations were performed by considering the aqueous solvent having a dielectric constant equal to 78.4. Water radius (R_{solv}) was set to 1.4 Å and the radius shift of water (δ^{SC}) was set equal to the water radius ($\delta^{SC} = R_{solv}$), as it is usually done.[16,19] The van der Waals radii of the Ca, C and O atoms were set to the standard values of 2.75, 1.70 and 1.52 Å, respectively.[20] The number of points per atom for the basic sphere used to build the solvent-accessible surface (SAS) was set to 974, whereas the number of segments per atom for the SAS was set to 110. A smoothing range of 0.1 Å

was used to ensure a continuous behavior of the energy surface. In order to estimate how our results are affected by the COSMIC parameters, the calculations were also performed by considering (i) $\delta^{SC} = R_{solv} = 1$ Å and (ii) the default van der Waals radii implemented in GULP: 2.75, 1.53 and 1.36 Å for Ca, C and O, respectively (see Table S1 in the Supporting Information).

2.1 Surface geometry optimization

All the surfaces were studied by using the 2D-slab model.[21] Slabs of varying thickness were generated by separating the bulk structure along the *hkl* plane of interest. Calculations were performed by considering the original 1×1 surface cell and the slab partitioned into two regions:

- region 1, containing both the surface and the underlying layers that are allowed to relax;
- region 2, having the same number of layers as region 1 and containing the rest of the slab material where no relaxation, with respect to the bulk crystal structure, is assumed to occur.

Calculations were done by considering slabs with thickness up to sixteen layers (eight for each region), which are sufficient to reproduce bulk-like properties at the centre of the slab and to obtain a careful description of the surface. GULP output files listing lattice parameters and atomic coordinates of the optimized dry and solvated slabs are freely available at http://mabruno.weebly.com/download.

Bulk and slab geometry optimizations were performed by means of the Newton-Raphson method and were considered converged when the gradient tolerance and the function tolerance (*gtol* and *ftol* adimensional parameters in GULP) were smaller than 0.0001 and 0.00001, respectively.

2.2 Twin interface geometry optimization

To investigate the (110) twin boundary, a 2D-slab model was adopted.[21] A twinned slab (bi-crystal), made by the slabs P and T, was generated in the following way:

(i) the slab P of a given thickness was made by cutting the bulk structure parallel to the 110 twin plane;

(ii) the slab T was made by applying the appropriate twin law (mirror plane parallel to the 110 one) to the atomic coordinates of the slab P.

Then, the twinned slab geometry (atomic coordinates) was optimized by considering all the atoms free to move. The calculation was done by considering the original 1×1 surface cell and the (110) twinned slab with thickness up to forty layers, which are sufficient to obtain an accurate description of the twinned interface. The slab thickness is considered appropriate when the relaxation of the outermost layers of the twinned slab does not affect the equilibrium geometry of the twin boundary

interface or, in other words, when the bulk-like properties are reproduced at the centre of the slabs P and T.

GULP output file listing lattice parameters and atomic coordinates of the optimized twinned slab is freely available at http://mabruno.weebly.com/download.

2.3 Calculation of surface and attachment energies at 0K

According to the standard two-regions strategy[22] employed by GULP, surface energy (γ_{hkl}) values were found starting from the energy of the surface block (U_s, region 1) and the energy of a portion of bulk crystal (U_b, region 2) containing the same number of atoms as the surface block. Both energies have been referred to A_{hkl}, the common surface area of the primitive unit cell:

$$\gamma_{hkl} = (U_s - U_b) / A_{hkl} \quad (1)$$

Evaluating the surface energy values and successively applying the Gibbs-Wulff theorem[23] allows to draw the theoretical equilibrium shape (ES) of a crystal.

On the contrary, the attachment energy, E_{att}^{hkl}, is needed to predict the theoretical growth shape of a crystal. This is the energy released when a stoichiometric layer of material is added on to the surface cut:

$$E_{att}^{hkl} = U_{tot}^{n+1} - U_{tot}^{n} - U_{tot}^{1} \quad (2)$$

where U_{tot}^{n} represents the total internal energy of a surface model consisting of n growth layers, and U_{tot}^{1} is the energy of the growth layer alone. The calculation of this exothermic quantity is obtained from the interaction energy of the growth layer at the surface with the rest of the underlying structure.

2.4 Twinning energy

The twinning energy, γ_{TE} (J/m^2), is the excess energy required to form a unit area of the twin boundary interface and reads:

$$\gamma_{TE} = \frac{E_T - E_{NT}}{A_{hkl}} \quad (3)$$

where E_T and E_{NT} are the energies of the optimized twinned and not twinned slabs, respectively. As for the equilibrium geometry, a twinned slab thickness of forty layers is sufficient to reach convergence on γ_{TE}.

3. Results and discussion

The initial crystal structure (space group *Pmcn*; a_0 = 4.9614, b_0 = 7.9671, c_0 = 5.7404 Å; $\alpha = \beta = \gamma = 90°$)[1] was allowed to relax, giving a_0 = 4.9609, b_0 = 7.9936, c_0 = 5.7020 Å and $\alpha = \beta = \gamma = 90°$. The crystal was then cut taking inspiration from Aquilano et al. (1997)[15] who classified the crystallographic forms of aragonite by the occurrence frequency derived from Goldschmidt.[24] The investigated surfaces are (100), (010), (001), (110), (101), (011), (111), (102), (012), (021), (112), (121), (122), (031) and (130). The (010) and (110) are cleavage planes, while the (110) is a common twin plane as well, giving lamellar twins parallel to the z axis or repeated twins leading to pseudo-hexagonal crystals.

Apart from the (100), each surface can be cut in more than one way, resulting in planes terminated by either calcium or carbonate ions; it is necessary to point out that we used for this work identifying the coordinates of each carbonate group with those of its central carbon.

It is important to stress that our calculations were carried out at 0K by considering an *implicit* aqueous solvent rather than *explicit* water molecules. This work can be considered as a preliminary study on the structural modifications of the main aragonite surfaces due to solvation. For a more reliable treatment, MD simulations at T > 0K should be performed. In this way, it should be possible to accurately investigate the structural reorganization of the surfaces in contact with water molecules and to take into account the possible ions tendency to dissolve into the solvent. However, in an our previous work carried out by means of the COSMIC strategy and Rohl potential on calcite surfaces at 0K,[11] we obtained structural modifications of the surfaces in good agreement with those experimentally observed in water. Therefore, we consider the COSMIC method able to reproduce the surface structural modifications.

3.1 Structure of surfaces

Here, we focus our attention on the structural modifications at T=0K due to geometry optimization both in vacuo and in the presence of the solvent. In particular, we analyze the relaxed surface structures of the {011}, {112}, {110}, {102}, {010}, {121} and {101}, that is the forms entering the equilibrium shape of the crystal, as discussed in the next paragraph. The equilibrium

geometries were drawn and reported in the Supporting Information (Figures S1-S14); the calculation output files are freely available at http://mabruno.weebly.com/download.

In order to do this, we examine how the z-coordinates of the uppermost Ca ions and CO_3 groups move when the most stable surfaces relax (see Table 1). On the (011) face, the Ca atom in the outermost layer is found to relax into the surface by 0.309 Å in vacuo and 0.261 Å in water, while the C atom relaxes out of the surface by 0.025 and 0.031 Å in the absence and in the presence of the solvent, respectively.

On the (110) and (010) surfaces, the highest relaxation for calcium is observed both in vacuo and in water. In fact, the Ca atom relaxes into the surfaces by 0.391 and 0.394 Å in vacuo and by 0.400 and 0.388 Å in water, respectively. On the other hand, the (110) C atom moves outward by 0.109 Å in vacuo and by 0.120 Å in water. The corresponding values for the wet (010) C atom are 0.045 and 0.047.

The lowest relaxation values related to calcium ions are registered for the (112) and (121) surfaces. The calculated displacements are always towards the inner bulk. In detail: 0.242 and 0.182 Å for the first surface and 0.236 and 0.176 for the second, without and with the solvent effect respectively. The carbon atoms, in contrast, tend to move outward the surfaces: by 0.059/0.062 and 0.172/0.154 for the vacuum/water cases in the (112) and (121), respectively.

The strongest changes in the C atom position concern the (102) and (101) faces: such ion move outward by 0.220 and 0.194 Å for the first surface, and by 0.264 and 0.246 Å for the second, without and with water respectively. On the contrary, the Ca ions tend to move inward by 0.328/0.286 and 0.344/0.307 for the vacuum/water cases in the (102) and (101), respectively.

Table 1. Ions displacements on the surfaces belonging to the seven crystallographic forms that enter the final equilibrium morphology of aragonite. Positive and negative values refer to movements inward and outward the surfaces, respectively.

surface	cut	Ca			CO_3		
		Δ_d	Δ_w	$\Delta_w - \Delta_d$	Δ_d	Δ_w	$\Delta_w - \Delta_d$
(0 1 1)	3	0.309	0.261	-0.047	-0.025	-0.031	-0.005
(1 1 2)	3	0.242	0.182	-0.060	-0.059	-0.062	-0.003
(1 1 0)	2	0.391	0.400	0.009	-0.109	-0.120	-0.011
(1 0 2)	2	0.328	0.286	-0.041	-0.220	-0.194	0.026
(0 1 0)	1	0.394	0.388	-0.006	-0.045	-0.047	-0.002
(1 2 1)	2	0.236	0.176	-0.061	-0.172	-0.154	0.018
(1 0 1)	1	0.344	0.307	-0.036	-0.264	-0.246	0.019

Looking at the data reported in Table 1, one can easily deduce that in vacuo relaxation drive Ca ions towards the internal structure, while carbonate groups are moved outwards. By adding water

molecules, calcium results to be slightly attracted outwards, except for the (110) surface. A stronger attraction outside the surface is calculated as well for the carbonate groups belonging to the (011), (112), (110) and (010) faces.

The {011}, {112}, {110}, {102}, {010}, {121} and {101} surface structures are only slightly affected by the COSMIC parameters. Indeed, by performing the structure optimizations with (i) $\delta^{SC} = R_{solv} = 1$ Å and with (ii) $\delta^{SC} = R_{solv} = \delta^{SC} = 1.4$ Å (both with van der Waals radii of Ca, C and O equal to 2.75, 1.53 and 1.36 Å, respectively), we observe very weak variations of the z-coordinates of the uppermost Ca and C atoms, as recently registered on calcite by Bruno et al.[11]

3.2 Dry and wet surface energies

Table 2 reports data concerning all the forty-four cuts coming from the fifteen investigated crystallographic forms. One can read information about the single cut, the ionic species outcropping on the surface, the surface energies calculated in vacuo (γ_d) and in aqueous solvent (γ_w) with the related percent difference Δ defined as $(\gamma_w - \gamma_d) / \gamma_d$, and the attachment energies (E_{att}) calculated for dry surfaces. We only report and discuss the relaxed values of the surface energy, since, as demonstrated by Bruno et al.,[25] the unrelaxed surface energies calculated at empirical level are physically ungrounded for another polymorph of calcium carbonate: the calcite.

Table 2. Termination, anhydrous (γ_d) and hydrated (γ_w) surface energy values, energy difference percentage between anhydrous and hydrated surface energies, Δ(%), and attachment energies (E_{att}) of dry surfaces belonging to the main crystal forms of aragonite are reported. Calculations were performed at T=0K using the Rohl et al.[17] carbonates force field and the COSMIC method[16] using the following parameters: $\delta^{SC} = R_{solv} = 1.4$ Å and van der Waals radii for Ca, C and O atoms equal to 2.75, 1.70 and 1.52 Å, respectively. The underlined indexes refer to the cuts characterizing the final ES. Bold energy values are the lowest among cuts belonging to the different crystallographic forms. The γ_d and γ_w data calculated by de Leeuw and Parker,[14] Akiyama et al.[13] and Sekkal and Zaoui[12] for some surfaces are reported as well. All the γ and E_{att} values are expressed in Jm^{-2} and kJ/mol, respectively.

form	cut	surface species	γ_d [this work]	γ_w [this work]	Δ (%)	E_{att} [this work]	γ_d[14]	γ_w[14]	γ_d[13]	γ_d[12]
{0 1 1}	1	CO_3	0.801	0.690	-13.9	-217.8	0.99	0.25	-	1.33, 1.20
{0 1 1}	2	CO_3	0.918	0.818	-10.9	-370.6	1.13	0.50	-	-
{0 1 1}	3	Ca	**0.578**	**0.527**	-8.8	**-125.6**	0.69	1.07	-	0.90, 0.84
{0 1 1}	4	Ca	1.219	0.991	-18.7	-345.0	1.16	1.15	-	1.09, 1.33
{1 0 2}	1	CO_3	0.635	0.570	-10.2	-345.6	-	-	-	-
{1 0 2}	2	Ca	**0.607**	**0.552**	-9.1	**-331.5**	-	-	-	-
{1 1 2}	1	CO_3	0.815	0.730	-10.4	-548.3	-	-	-	-
{1 1 2}	2	CO_3	0.972	0.824	-15.2	-786.5	-	-	-	-
{1 1 2}	3	Ca	**0.612**	**0.543**	-11.3	**-386.5**	-	-	-	-
{1 1 2}	4	Ca	0.820	0.721	-12.1	-709.3	-	-	-	-
{1 1 0}	1	CO_3	0.797	0.761	-4.5	-657.1	1.04	0.81	0.73	1.30, 0.92
{1 1 0}	2	Ca	**0.730**	**0.693**	-5.1	**-218.3**	0.88	0.56	0.64	1.03, 0.73
{1 2 2}	1	Ca	0.784	**0.664**	-15.3	-651.9	-	-	-	-

{1 2 2}	2	Ca	0.829	0.732	-11.7	-668.1	-	-	-	-
{1 2 2}	3	CO_3	0.847	0.782	-7.7	**-556.3**	-	-	-	-
{1 2 2}	4	CO_3	**0.730**	0.680	-6.8	-721.2	-	-	-	-
{1 0 1}	1	Ca	**0.752**	**0.682**	-9.3	**-479.9**	0.99	0.53	-	1.19, 0.90
{1 0 1}	2	CO_3	0.856	0.772	-9.8	-781.8	1.08	0.62	-	1.31, 1.00
{1 1 1}	1	CO_3	**0.760**	**0.684**	-10.0	**-344.1**	0.84	0.64	-	1.09, 0.83
{1 1 1}	2	CO_3	0.875	0.787	-10.1	-527.2	1.02	0.72	-	-
{1 1 1}	3	Ca	1.040	0.965	-7.2	-636.8	1.40	1.03	-	1.30, 0.94
{1 1 1}	4	Ca	0.877	0.787	-10.3	-466.3	1.03	0.79	-	-
{0 1 2}	1	Ca	0.886	0.779	-12.1	**-596.1**	-	-	-	-
{0 1 2}	2	Ca	**0.767**	**0.726**	-5.3	-1227.6	-	-	-	-
{0 1 2}	3	CO_3	1.188	0.993	-16.4	-612.4	-	-	-	-
{0 1 2}	4	CO_3	1.128	1.027	-9.0	-883.2	-	-	-	-
{0 0 1}	1	CO_3	**0.779**	**0.721**	-7.4	**-257.9**	0.85	0.90	0.58	1.01, 0.78
{0 0 1}	2	Ca	1.077	1.044	-3.1	-524.3	1.05	0.62	0.89	1.59, 1.36
{1 2 1}	1	CO_3	0.866	0.773	-10.7	-636.3	-	-	-	-
{1 2 1}	2	CO_3	**0.797**	**0.723**	-9.3	**-564.2**	-	-	-	-
{1 2 1}	3	Ca	0.822	0.753	-8.4	-660.2	-	-	-	-
{0 2 1}	1	CO_3	1038	0.868	-16.4	**-464.4**	-	-	-	-
{0 2 1}	2	Ca	**0.803**	**0.745**	-7.2	-793.8	-	-	-	-
{0 2 1}	3	CO_3	1.416	1.265	-10.7	-669.5	-	-	-	-
{0 2 1}	4	Ca	0.971	0.896	-7.7	-639.5	-	-	-	-
{0 1 0}	1	Ca	**0.808**	**0.749**	-7.3	**-241.8**	0.96	0.24	0.73	1.14, 0.80
{0 1 0}	2	CO_3	0.868	0.821	-5.4	-600.6	1.50	1.77	0.84	1.57, 1.10
{1 3 0}	1	CO_3	0.978	**0.847**	-13.4	-1013.5	-	-	-	-
{1 3 0}	2	Ca	**0.956**	0.878	-8.2	**-792.4**	-	-	-	-
{0 3 1}	1	Ca	**0.984**	**0.915**	-7.0	-1102.2	-	-	-	-
{0 3 1}	2	CO_3	1.081	1.011	-6.5	**-985.5**	-	-	-	-
{0 3 1}	3	Ca	1.075	0.985	-8.4	-997.1	-	-	-	-
{0 3 1}	4	CO_3	1.093	0.985	-9.9	-1024.3	-	-	-	-
{1 0 0}		Ca/CO_3	**1.028**	**0.900**	-12.5	**-840.7**	1.50	0.93	-	1.71, 1.23

The {011} has four different cuts: two Ca-terminated and two CO_3-terminated. Their surface energy values vary from 0.578 Jm^{-2} (the lowest for aragonite) to 1.219 Jm^{-2} both for Ca-terminated surfaces. In the presence of water molecules, the γ of the most stable surface reduces to 0.527 Jm^{-2}, with a delta of -8.8%.

The {112} has four different cuts as well: again two Ca-terminated and two CO_3-terminated. Their γ values vary from 0.612 Jm^{-2} for a Ca-terminated surface to 0.972 Jm^{-2} for a CO_3-terminated one. With solvation, the lowest energy value moves to 0.543 Jm^{-2} reducing by 11.3%.

The {110} has two different cuts with the two different terminations. The Ca-terminated one is the most stable with a γ value of 0.730 Jm^{-2}, while 0.797 Jm^{-2} is the value for the CO_3-terminated surface. The energies of the same morphological cuts become 0.693 and 0.761 Jm^{-2} after hydration.

The {102} has two different cuts with the two different terminations. The Ca-terminated one is the most stable with a gamma value of 0.607 Jm^{-2}, while 0.635 Jm^{-2} is the value for the CO_3-terminated surface. With solvation, we obtain 0.552 and 0.570 Jm^{-2}, respectively.

The {010} has two different cuts with the two different terminations. The Ca-terminated one is the most stable with a gamma value of 0.808 Jm^{-2}, while 0.868 Jm^{-2} is the value for the CO_3-terminated surface. Such energies reduce to 0.749 and 0.821 Jm^{-2} considering the effect of the water molecules.

The {121} has three different cuts as well: two CO_3-terminated and one Ca-terminated. The lowest γ values are of a CO_3-terminated one: 0.797 and 0.723 Jm^{-2} for anhydrous and hydrated conditions, respectively.

The {101} has two different cuts with the two different terminations.. The Ca-terminated one is the most stable with a gamma value of 0.752 Jm^{-2}, while 0.856 Jm^{-2} is the value for the CO_3-terminated surface; after a lowering by 9.3%, the lowest energy surface results to be affected by the presence of water, its γ_w reaching 0.682 Jm^{-2}.

As expected, all the γ_w values are lower than the equivalent γ_d, this is due to stabilization of the interface by the solvent. Besides, as calculated for calcite by Bruno et al.,[11] one can observe a slight decrease of the surface energies, the average reduction related to the most stable cuts being 9.2±2.9%. The highest reduction is observed for one cut of the (011) face (18.7%), whereas the lowest one is found for a (110) cut (4.5 %).

As already mentioned, we recalculated the solvated surface energies by considering: (i) R_{solv} = δ^{SC} = 1 and van der Waals radii of Ca, C and O equal to 2.75, 1.53 and 1.36 Å, respectively, and (ii) R_{solv} = δ^{SC} = 1.4 with the same van der Waals radii. All the related results are reported in Table S1 (Supporting Information). Here, it is noteworthy pointing out that changes in the equilibrium morphology are negligible, since γ_w values undergo a somewhat homogeneous variation: in the case (i) we have an average reduction of 13.5±3.7% with respect to the dry values, whereas in the case (ii) the average reduction is 10.2±3.9%. This demonstrates that the solvated ES of aragonite at 0K is not affected by the COSMIC parameters.

As a comparison, Table 2 reports as well the dry and wet surface energies calculated by de Leeuw and Parker,[14] and the dry surface energies calculated by Akiyama et al.[13] at DFT level and Sekkal and Zaoui[12] at empirical level (by using both the Raiteri et al.[26] and Xiao et al.[27] force fields) for some of the forms we investigated. It is necessary to point out that it is not possible to make direct comparison between our and the de Leeuw and Parker's results as the authors do not provide detailed structural information about the surface cuts they have considered. Nevertheless, looking at

the ion termination, the dry energy values seem to follow the same trend even if our values are generally lower. For what concerns the γ_w, as better examined later in the paragraph, our values do not move away too much from the γ_d case as in the work by de Leeuw and Parker. Furthermore, it is essential to underline that our γ_d values are more concordant with Akiyama and coworkers' ab initio calculations, even if these authors focused their attention only on the few cuts originating from the {001}, {110} and {010} forms.

Instead, as it concerns the Sekkal and Zaoui's results,[12] it is important to stress here that they performed the calculations by using the recent calcite's force fields developed by Raiteri et al.[26] and Xiao et al.,[27] which were designed to reproduce the thermodynamics of the aqueous calcium carbonate system at room temperature within molecular dynamics simulations and not to reproduce the properties of the dry crystal surfaces at 0K. For this reason we believe that the dry surface energy values obtained by Sekkal and Zaoui[12] are not reliable and, therefore, not comparable with our and previous estimates.

By applying the Gibbs–Wulff's theorem[23] and considering the surface energy values in Table 2, we drawn the solvated and dry equilibrium shape at 0K (Figure 1). The seven crystallographic forms that enter the vacuum equilibrium morphology are the same registered in water. One, for accurately studying the few differences occurring between the dry shape and the solvated one, can take into account the morphological relevance index MRI for all the {hkl} forms, defined as the percent ratio between the total area of the faces belonging to a {hkl} form and the total surface area of the crystal. It is noteworthy that the solvent effect is rather moderate. The morphological relevance order for the anhydrous shape is {011}, {112}, {110}, {102}, {010}, {121} and {101}, having MRIs of 31.4, 25.7, 24.4, 10.6, 5.5, 1.4 and 1.0%, respectively. The morphological relevance order for the hydrated shape changes to {112}, {011}, {110}, {102}, {010}, {121} and {101}; the MRIs are 35.6, 28.8, 19.5, 5.8, 5.2, 3.5 and 1.7%, respectively. Here, some considerations:

- water slightly lowers the MRI of the stable {011} dry form;
- solvent act more strongly on the {112} form which, as a consequence, becomes more relevant than the {011} in the final solvated morphology;
- the {110} and {102} MRIs reduce by ~5% after solvation, while there are not substantial MRI variations for the {010}, {121} and {101}.

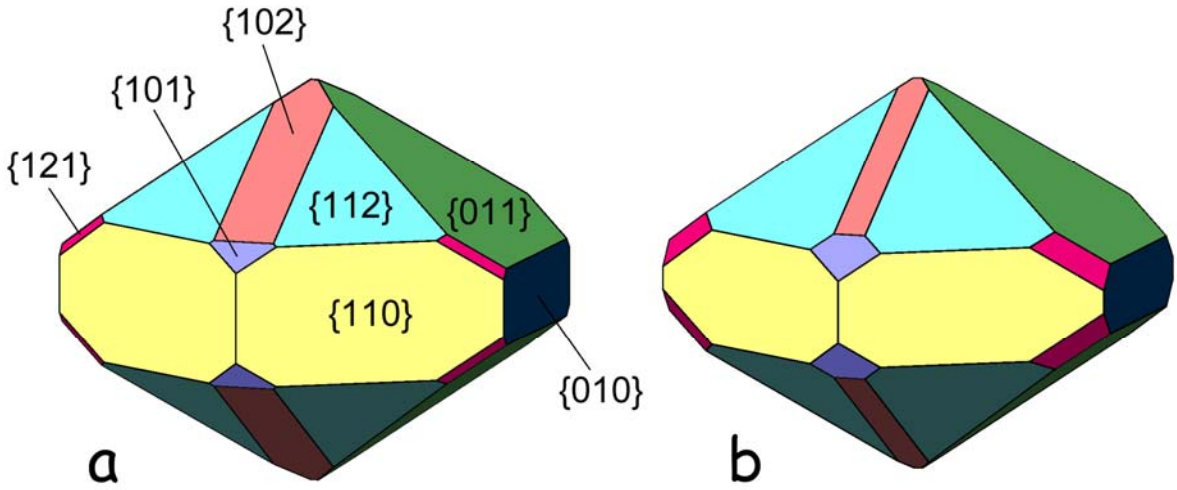

Figure 1. (a) Dry and (b) solvated equilibrium shape of aragonite at 0K.

The relative MRIs allow to estimate the weighted value, $\gamma^{d}_{weighted} = \left(\sum A_{hkl} \cdot \gamma^{d}_{hkl}\right) / \sum A_{hkl}$ = 0.644 Jm^{-2}, of the athermal relaxed surface energy of aragonite in vacuo; A_{hkl} is the surface area of the {hkl} form. This value is reduced by -8.8%, being $\gamma^{w}_{weighted} = \left(\sum A_{hkl} \cdot \gamma^{w}_{hkl}\right) / \sum A_{hkl}$ = 0.587 Jm^{-2}, when taking into account the hydration. It is worth considering this is not so a sensible difference when predicting the 3D nucleation frequency of aragonite, even if one should look at a more realistic ES, in which configurational and vibrational entropies are taken into account.

Finally, we calculated for each surface cut the attachment energies in vacuo and at T=0K as well (see Table 2). Looking at the results we can conclude that the {011}, {110}, {010} and {001} forms are expected to be the most relevant in controlling the growth morphology, their E_{att} being equal to -125.6, -218.3, -241.8 and -257.9 kJ/mol, respectively.

3.3 The (110) twin boundary interface

The equilibrium geometry of the (110) twin boundary interface obtained with the force field method is reported in Figure 2. According to the (110) twin law, the two parts of the twin are related by a mirror parallel to the 110 plane. The latter is also named “original composition plane”: OCP, a lattice plane on which a stacking fault of growth units in twinned position may occur at some stage of the growth.[28,29]

Before to describe the structural modifications induced by the presence of the twin boundary interface, we define the positions of atoms in the bi-crystal (twinned slab) by expressing them in the common orthogonal base: the axis are [001] perpendicular to Y which, in turn, coincides with

[110]; Z is parallel to the reciprocal vector $-\tau_1^* + \tau_2^*$. The transformation matrix from the standard ortonormal reference to the one chosen is:

$$\begin{pmatrix} 0 & 0 & 1 \\ \frac{a_0}{\sqrt{a_0^2+b_0^2}} & \frac{b_0}{\sqrt{a_0^2+b_0^2}} & 0 \\ \frac{-b_0}{\sqrt{a_0^2+b_0^2}} & \frac{a_0}{\sqrt{a_0^2+b_0^2}} & 0 \end{pmatrix} \quad (4)$$

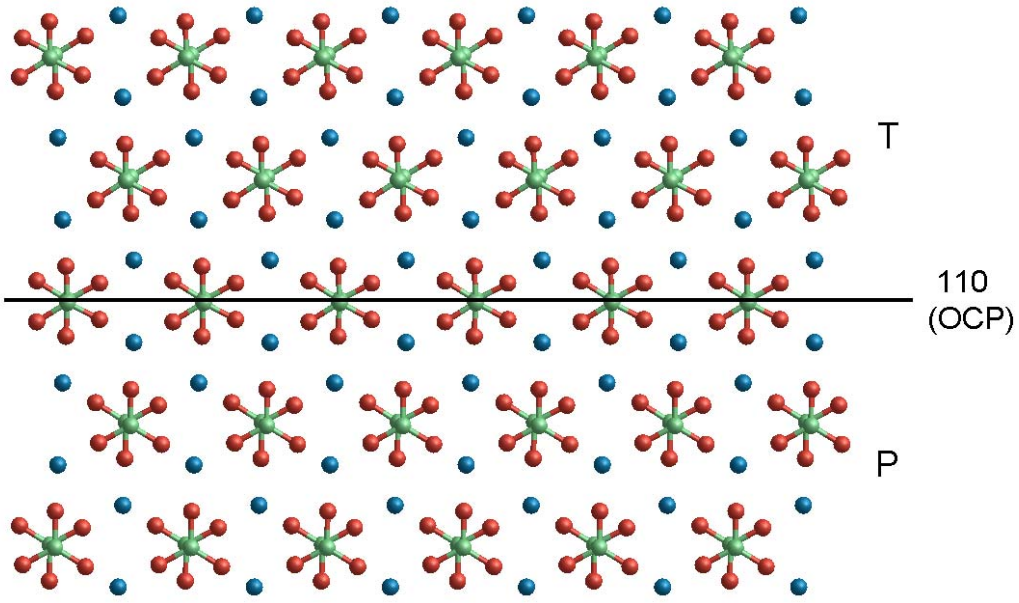

Figure 2. [001] view of the equilibrium geometry of the (110) twin boundary interface. The solid black line is the 110 plane (the original composition plane, OCP).

Then, in order to describe the expansion (relaxation) of the interface between the two crystals (P and T) composing the twinned slab, variables Δ_3^l are defined as follows. Let be:

$$X_3^{lk} = n_k^{-1} \sum_{i=1}^{n_k} x_3^{lk} \quad (5)$$

where x_3^{lk} are the atomic coordinates measured along [-1 1 0], the index k designates the atom species, l the layer number within the column representing the repeat 3D cell generating the twinned slab by translation, n_k the number of atom of specie k in every layer l.

The X_3^{lk} are then lumped together in a collective variable, C_3^l, expressing the mean coordinates associated to layer l:

$$C_3^l = \frac{1}{3}\sum_{K=1}^{3} X_3^{lk} \quad (6)$$

Finally $\Delta_3^l = C_3^{l+1} - C_3^l$ represents the translation in the Z direction of layer $l+1$ in respect to l. Due to the 2D periodic boundary conditions, no lattice deformations occurs in 110 planes; the fractional coordinates of the C atoms laying on the OCP, are intermediate between those in the T and P crystals. Δ_3^l values representing mean relative layers translations in direction Z, then $\frac{\Delta_3^l}{d_{020}}$ values correspond to the layer decomposition (some example are reported in the paper by Müller and Saul[30]) of the intrinsic strain due to the interface relaxation as discussed in the following.

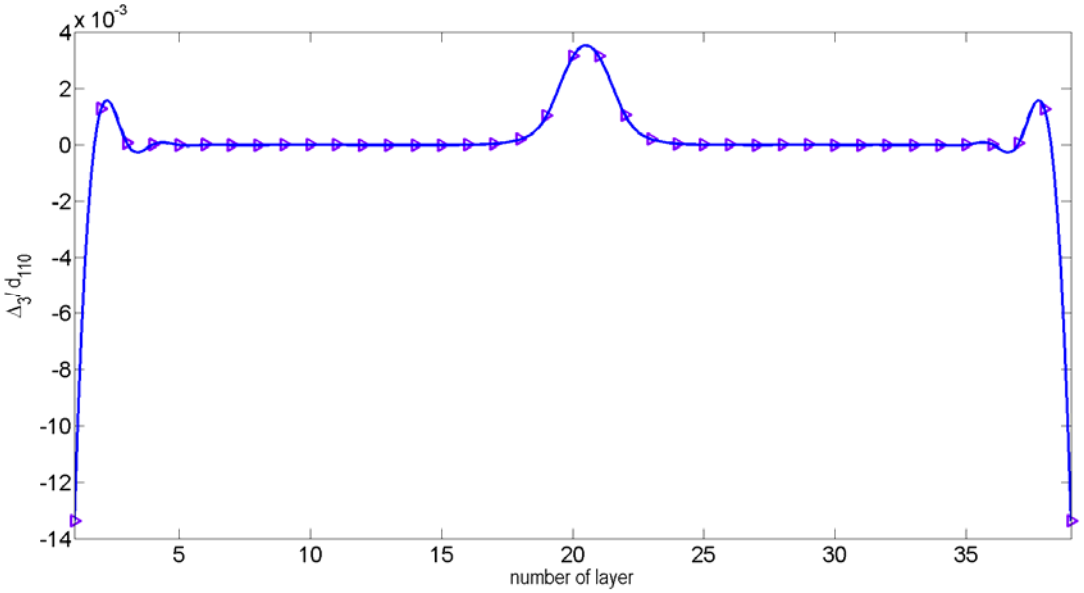

Figure 3. Distribution of normal strain in the slab, from the surface of the parent to that of the twinned crystal.

The interface deformations caused by the breaking of the symmetry of the forces through the interface, correspond to a new equilibrium characterized by an excess energy of the bi-crystal: the

twinning energy, which is calculated by means of eq. (3) and results to be 0.017 Jm^{-2}. A component of this excess can be ascribed to the elastic energy associated to the interface intrinsic strain in direction Z, represented in Fig.3.

The mean elastic energy, in matrix notation, is:

$$E_e = \frac{1}{2} V \frac{\sum_i \sigma_i \varepsilon_i}{N_l} \quad (7)$$

where V is the volume of a non deformed cell and σ_i, ε_i are the stress and strain tensors calculated in every cell. In order to estimate the stress tensor we use, as an approximation to the slab elastic constants, those measured and reported by Liu et al.[31]

The summation is over the number of cells in the slab close to the interface between the two twinned crystals. The strain is measured with reference to the non deformed crystal. In the case of aragonite, the estimated mean elastic energy, E_e, amounts to about 4% of the twinning energy, 6.8×10^{-4} Jm^{-2}.

We cannot perform a finer analysis for, as shown by Dingreville et al.,[32] the accurate evaluation of the distribution of the stress in the layers requires the calculation of the derivatives of the energy of the twin in respect to the inter-atomic distances. As a matter of fact, in an our previous work on gypsum (010) penetration twin[33] the calculated stress perpendicular to the surface layers is not nil, as required by the equilibrium in the absence of bulk forces. One can suppose that at the twin interface the stress is inhomogeneous, however the calculation performed are not satisfactory to describe this situation. To assess the stress distribution in twins will be the object of future works.

4. Conclusions

In this work we determined at empirical level the equilibrium geometry at 0K of the (i) (100), (010), (001), (110), (101), (011), (111), (102), (012), (021), (112), (121), (122), (031) and (130) surfaces of aragonite, both in dry and solvated conditions, and (ii) (110) twin boundary interface. Furthermore, the dry and solvated surface energies at 0K of the (100), (010), (001), (110), (101), (011), (111), (102), (012), (021), (112), (121), (122), (031) and (130) faces were calculated, as well as the (110) twinning energy at 0K.

The entire work let us to deduce some general conclusions:

(i) In vacuo relaxations differently drive the two ionic species involved in aragonite crystal surfaces: the Ca ions result to be more attracted towards the bulk crystal while the CO_3 groups outwards; by considering water on the surfaces, Ca ions result to be generally less attracted inwards, while the CO_3 ions behavior depends on the crystal face.

(ii) Surface energies decrease in the presence of the aqueous solvent. The relaxation degree after solvation vary from a few percent units up to a maximum of 18.7% for one of the high energy cuts of the (011) surface. Taking into account the most stable cuts, an average of 8.3±2.0% is registered. Such a small reduction of the γ after hydration originates weak differences in the final equilibrium shape.

(iii) Among the surfaces that enter the final ES, calculations demonstrate that each cut which has the lowest energy in vacuo, has the lowest energy in hydrated conditions as well.

(iv) By excluding the {121} form, the typical surfaces of the ES are characterized by a calcium ions termination.

(v) By analyzing the modeled crystalline surfaces before and after geometry optimization, one can observe that all the CO_3-terminated cuts have a common feature: the carbonate groups tends to rotate in order to lie flat on the surfaces, as a relaxation result. This behavior was already observed by de Leeuw and Parker.[14]

(vi) We estimated very low values for twinning energy (0.017 Jm^{-2}) and elastic energy (6.8×10^{-4} Jm^{-2}), this latter being stored by the twinned crystal as a consequence of the interface strain. These very low values are due to the strong similarity among the equilibrium structure of the 110 twin and that of the normal crystal (see Figure 2). The same relation between energy and structure was observed for the (0001) contact twin of calcite[34,35] and (100)[36,37] contact twin of gypsum ($CaSO_4\cdot2H_2O$), where the following twinning energies were estimated: 0.001-0.047 and 0.014 Jm^{-2}, respectively. From a genetic point of view, the lower is the twinning energy the higher is the probability to obtain a twinned crystal. Then, the extremely low value of the twinning energy we obtained allows to explain the facility of formation of aragonite twinned crystals. Indeed, according to the classical nucleation theory, the lower is the twinning energy the lower is also the supersaturation of the mother solution (from which the crystals nucleate) for overcoming the nucleation barrier to form twinned crystals.

Here, it is important to stress that our estimate of twinning energy was obtained at 0 K. In order to calculate the twinning energy a $T > 0$ K, it is necessary to take into account the vibrational motion of atoms (vibrational entropy). This is a thermodynamical quantity that may affect slightly the values of γ_{TE}, as it depends on the difference of entropy between a twinned crystal and a perfect one.

(vii) The tabular habit of aragonite crystals in nacre may be: (a) a *growth habit*, which is a consequence of the lower growth rate of the {001} faces with respect to that of the other crystallographic forms, or (b) an *equilibrium habit*, where the somewhat different shape of the crystal with respect to that we calculated, is due to the different energies of the interfaces between the crystal faces and the organic environment in which the crystal nucleates and grows. However, in both cases, there is a strong affinity (likely also an epitaxial relationship) between the organic matter and the {001} form of aragonite.

Supporting Information Available. Drawings of the optimized geometries of the {011}, {112}, {110}, {102}, {010}, {121} and {101} forms entering into the equilibrium shape of aragonite at 0K (Figures S1-S14). Dry and solvated relaxed surface energies at 0K of the main faces of aragonite ({011}, {102}, {112}, {110}, {122}, {101}, {111}, {012}, {001}, {121}, {021}, {010}, {130}, {031} and {100}) (Table S1) calculated by means of the Rohl et al.[17] force field and by considering different COSMIC parameters: (i) $R_{solv} = \delta^{SC}$ =1, r(Ca) = 2.75 Å, r(C) = 1.53 Å, r(O) = 1.36 Å; (ii) $R_{solv} = \delta^{SC}$ =1.4, r(Ca) = 2.75 Å, r(C) = 1.53 Å, r(O) = 1.36 Å; (iii) $R_{solv} = \delta^{SC}$ =1.4, r(Ca) = 2.75 Å, r(C) = 1.70 Å, r(O) = 1.52 Å; r(Ca), r(C) and r(O) are van der Waals radii of Ca, C and O, respectively. This material is available free of charge via the Internet at http://pubs.acs.org.

References

[1] de Villiers, J.P.R. *American Mineralogist* **1971**, *56*, 758-767.

[2] Jackson, A. P.; Vincent, J. F.V.; Turner, R. M. *Proc. R. Soc. B* **1988**, *234*, 415-440.

[3] Li, X. D.; Chang, W. C.; Chao, Y. J.; Wang, R. Z.; Chang, M. *Nano Lett.* **2004**, *4*, 613-617.

[4] Mukai, H.; Saruwatari, K.; Nagasawa, H.; Kogure, T. *Journal of Crystal Growth* **2010**, *312*, 3014-3019.

[5] Li, X.; Huang, Z. *Physical Reviews Letters* **2009**, *102*, 075502.

[6] Li, X. D.; Xu, Z. H.; Wang, R. Z. *Nano Lett.* **2006**, *6*, 2301-2304.

[7] Rousseaua, M.; Lopeza, E.; Stempfle, P.; Brendle, M.; Franked, L.; Guetted, A.; Naslaind, R.; Bourrat, X. *Biomaterials* **2005**, *26*, 6254-6262.

[8] Kudo, M.; Kameda, J.; Saruwatari, K.; Ozaki, N.; Okano, K.; Nagasawa, H.; Kogure, T. *J. Struct. Biol.* **2010**, *169*, 1-5.

[9] Wada, K. *Biomineralization* **1972**, *6*, 141–159.

[10] Bevelander, G.; Nakahara, H. *Calcif. Tissue Res.* **1969**, *3*, 84–92.

[11] Bruno, M.; Massaro, F.R.; Pastero, L.; Costa, E.; Rubbo, M.; Prencipe, M.; Aquilano, D. *Crystal Growth & Design* **2013**, *13*, 1170-1179.

[12] Sekkal, W.; Zaoui, A. *Sci. Rep.* **2013**, *3*, 1587.

[13] Akiyama, T.; Nakamura, K.; Ito, T. *Physical Review B* **2011**, *84*, 085428.

[14] de Leeuw, N.H.; Parker, S.C. *J. Phys. Chem. B* **1998,** *102,* 2914-2922.

[15] Aquilano, D.; Rubbo, M.; Catti, M.; Pavese, A. *Journal of Crystal Growth* **1997**, *182*, 168-184.

[16] Gale, J. D.; Rohl, A. L. *Molecular Simulation* **2007**, *33*, 1237-1246.

[17] Rohl, A. L.; Wright, K.; Gale, J. D. *Am. Miner.* **2003**, *88*, 921-925.

[18] Gale, J.D. *J. Chem. Soc. Faraday Trans.*, **1997**, *93*, 629-637.

[19] Klamt, A.; Schüürmann, G. *J. Chem. Soc. Perkin Trans.* **1993**, *2*, 799-805.

[20] Bondi, A. *The Journal of Physical Chemistry* **1964**, *68*, 441-451.

[21] Dovesi, R.; Civalleri, B.; Orlando, R.; Roetti, C.; Saunders, V. R. In *Ab Initio Quantum Simulation in Solid State Chemistry*; Lipkowitz, B. K., Larter, R., Cundari, T. R., Eds.; Reviews in Computational Chemistry, Vol. 21; John Wiley and Sons Inc.: New York, 2005; pp 1-125.

[22] Gale, J. D. General Utility Lattice Program User's Manual, Curtin University of Technology, Perth, Australia.

[23] Wulff, G. *Z. Kristallogr. Kristallgeom.***1901**, *34*, 949.

[24] Goldschmidt, V. *Atlas der Krystallformen*. Carl Winters Universitatsbuchabhandlung: Heidelberg 1913. Band 1, Text 90-104, Tafeln 966115.

[25] Bruno, M.; Massaro, F. R.; Prencipe, M.; Aquilano, D. *CrystEngComm* **2010**, *12*, 3626-3633.

[26] Raiteri, P.; Gale, J. D.; Quigley, D.; Rodger, P. M. *J. Phys. Chem. C* **2010,** *114,* 5997–6010.

[27] Xiao, S.; Edwards, S. A.; Gräter, F. *J. Phys. Chem. C* **2011**, *115*, 20067–20075.

[28] Hartman, P. *Z. Kristallogr.* **1956**, *107*, 225–237. Hartman, P. *Acta Crystallogr.* **1958**, *11*, 459–464. Hartman, P. In *Crystal Growth: An Introduction*; Hartman, P., Ed.; North Holland Publishing Co.: Amsterdam, 1973; pp 367-402.

[29] Curien, H; Kern, R. *Bull. Soc. Franc. Miner. Crist.* **1957**, *80*, 111–132.

[30] Müller, P.; Saul, A. *Surf. Sci. Rep.* **2004**, *54*, 157–258.

[31] Liu, L.; Chen, C.; Lin, C.; Yang, Y. *Phys. Chem. Minerals* **2005,** *32*, 97–102.

[32] Dingreville, R.; Qu, I. J. *Computational Materials Science* **2009***,46,* 83-91.

[33] Rubbo, M.; Bruno, M.; Massaro, F. R.; Aquilano, D. *CrystEngComm* **2013**, *15*, 958-964.

[34] Bruno, M.; Massaro, F. R.; Rubbo, M.; Prencipe, M.; Aquilano, D. *Crystal Growth & Design* **2010**, *10*, 3102-3109.

[35] Akiyama, T.; Nakamura, K.; Ito, T. *The Journal of Physical Chemistry C* **2012**, *116*, 987-993.

[36] Rubbo, M.; Bruno, M.; Aquilano, D. *Crystal Growth & Design* **2011**, *11*, 2351-2357.

[37] Rubbo, M.; Bruno, M.; Massaro, F. R.; Aquilano, D. *Crystal Growth & Design* **2012**, *12*, 264-270.

For Table of Contents Use Only

Surface structure, morphology and (110) twin of aragonite

Francesco Roberto Massaro[1] *Marco Bruno*[2] *Marco Rubbo*[2]

[1]Dipartimento di Geoscienze – Università di Padova, via G. Gradenigo 6, I-35131 Padova, Italy

[2]Dipartimento di Scienze della Terra - Università di Torino, via Valperga Caluso 35, I-10125 Torino, Italy.

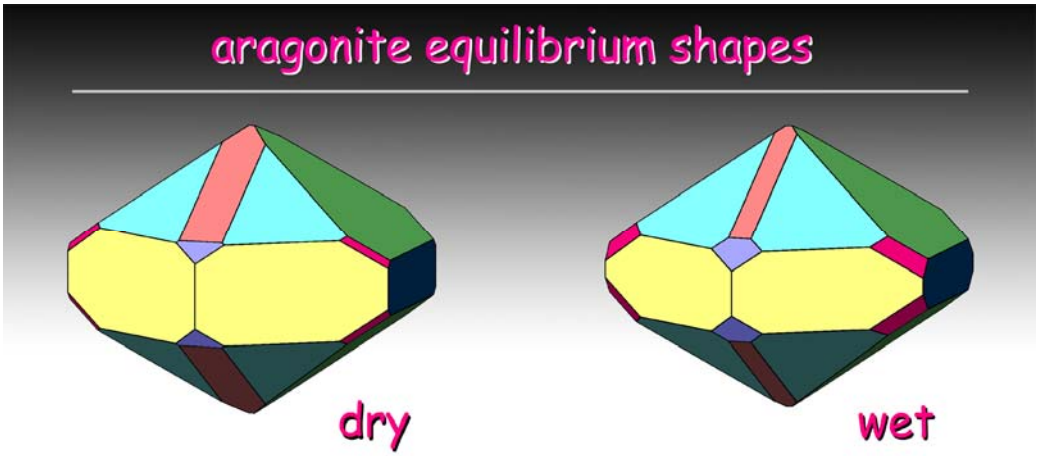

Synopsis

In order to better understand the growth mechanisms involving the aragonite in both geological and biological systems, a detailed study of its surfaces was performed. The dry and solvated surface energies at 0K of the crystal faces were calculated, as well as the (110) twinning energy and the interface elastic energy at 0K.